On the Cosmic Evolution of Fe/Mg in QSO Absorption Line Systems

Arjun Dey[1,2]*, Paul Torrey[3,4], Kate H. R. Rubin[5], Guangtun Ben Zhu[6,7], Joshua Suresh[5]

[1] *National Optical Astronomy Observatory, Tucson, AZ 85726*
[2] *Fellow, Radcliffe Institute for Advanced Study, Harvard University, Byerly Hall, 8 Garden Street, Cambridge, MA 02138*
[3] *TAPIR 350-17, California Institute of Technology, 1200 E. California Boulevard, Pasadena, CA 91125, USA*
[4] *MIT Kavli Institute for Astrophysics & Space Research, Cambridge, MA, 02139*
[5] *Harvard-Smithsonian Center for Astrophysics, 60 Garden Street, Cambridge, MA 02138*
[6] *Department of Physics & Astronomy, Johns Hopkins University, 3400 N. Charles Street, Baltimore, MD 21218, USA*
[7] *Hubble Fellow*

11 June 2015

ABSTRACT

We investigate the variation of the ratio of the equivalent widths of the FeIIλ2600 line to the MgII$\lambda\lambda$2796,2803 doublet as a function of redshift in a large sample of absorption lines drawn from the Johns Hopkins University - Sloan Digital Sky Survey Absorption Line Catalog. We find that despite large scatter, the observed ratio shows a trend where the equivalent width ratio $\mathcal{R} \equiv W_{\mathrm{FeII}}/W_{\mathrm{MgII}}$ decreases monotonically with increasing redshift z over the range $0.55 \leq z \leq 1.90$. Selecting the subset of absorbers where the signal-to-noise ratio of the MgII equivalent width W_{MgII} is ≥ 3 and modeling the equivalent width ratio distribution as a gaussian, we find that the mean of the gaussian distribution varies as $\mathcal{R} \propto (-0.045 \pm 0.005)z$. We discuss various possible reasons for the trend. A monotonic trend in the Fe/Mg abundance ratio is predicted by a simple model where the abundances of Mg and Fe in the absorbing clouds are assumed to be the result of supernova ejecta and where the cosmic evolution in the SNIa and core-collapse supernova rates is related to the cosmic star-formation rate. If the trend in $\mathcal{R}$ reflects the evolution in the abundances, then it is consistent with the predictions of the simple model.

Key words: intergalactic medium; quasars: absorption lines; galaxies: halos, abundances, evolution

1 INTRODUCTION

The absorption lines of heavy elements (e.g., C, Mg, O, Fe) observed in the spectra of distant quasi-stellar objects (QSOs) provide one of the best ways of observing and understanding the evolving chemical enrichment of the Universe. Several lines of evidence suggest that these absorption lines arise in the circumgalactic medium (CGM) surrounding galaxies lying close to the lines of sight to QSOs (e.g., Bahcall & Spitzer 1969; Yanny et al. 1990; Bergeron & Boissé 1991; Steidel 1995; Zhu et al. 2014). The source of the heavy elements in the CGM is not clear, but it is thought to result from enrichment of the halo gas by large-scale galactic outflows driven by a combination of stellar winds, supernovae, active galactic nuclei (AGN)

and by the accretion of gas tidally stripped during mergers from star-forming galactic disks (e.g., Oppenheimer & Davé 2006; Dalla Vecchia & Schaye 2008; Suresh et al. 2015). The ubiquity of galactic winds associated with star-formation in galaxies over a wide range in redshift is now empirically well established (e.g., Weiner et al. 2009; Erb et al. 2012; Martin et al. 2012; Kornei et al. 2012; Rubin et al. 2014) by the detection of blue-shifted absorption lines of MgII and FeII in galaxies. These outflows can carry enriched material out of galactic disks to distances of $\gtrsim 50$ kpc into galaxy halos (Bordoloi et al. 2011; Rubin et al. 2014) and thus enrich the CGM (e.g., Prochaska et al. 2011). Outflows of enriched material from galaxy disks have also been invoked to regulate the mass-metallicity relationship observed in galaxies (e.g., Tremonti et al. 2004; Finlator & Davé 2008; Davé et al. 2011; Torrey et al. 2014): star-formation, fuelled by accreted gas, can increase a galaxy's metallicity, but out-

* E-mail: dey@noao.edu

flows can remove enriched gas from the galaxy and, in lower mass systems, prevent further star-formation and enrichment (e.g., Mannucci et al. 2010).

In this picture the metal enrichment of the circumgalactic medium is the result of supernovae and a natural consequence is that the ratio of α elements to Fe should reflect (to first order) the relative rates of core collapse supernovae (CCSN; which result from the explosion of a massive star) and Type Ia supernovae (SNIa; which result from the explosion of an accreting white dwarf). The heavy element yields from both classes of supernovae have been modeled in various studies (Nomoto et al. 1997; Thielemann et al. 2003), which typically find that the α-elements are formed predominantly in CCSN, whereas Fe production is dominated by SNIa. The observed ratio of α-element to Fe equivalent widths in the spectra of absorption line systems over a range of redshifts can potentially provide an important window into the relative variation of SN rates, the efficiency of outflows in enriching the CGM, and the resultant abundance patterns of diffuse CGM and IGM material with cosmic time.

In this paper, we use the Johns Hopkins University - Sloan Digital Sky Survey (JHU-SDSS) Metal Absorption Line Catalog (Zhu & Ménard 2013, hereafter ZM13) to investigate the variation of the FeII/MgII ratio as a function of redshift. The catalog tabulates the equivalent widths for 35,752 absorption line systems measured in the spectra of QSOs observed by the Sloan Digital Sky Survey DR7 data release (Abazajian et al. 2009; York et al. 2000). We focus on the measurements of the equivalent widths of the MgII$\lambda\lambda 2796.35, 2803.53$ ($^2S \rightarrow {}^2P_{\frac{1}{2},\frac{3}{2}}$) and FeII$\lambda\lambda 2586.00, 2600.73$ ($a\,^6D_{\frac{9}{2}} \rightarrow z\,^6D_{\frac{7}{2},\frac{9}{2}}$) transitions (see, e.g., Prochaska et al. 2011; Hartigan et al. 1999).

We present the sample in §2 and our analyses in §3 and show that there is evidence for a trend of decreasing $W_{\mathrm{FeII}}/W_{\mathrm{MgII}}$ with redshift. In §4 we discuss the possible origins of this trend. We consider the caveats and whether the ratio is a viable proxy for understanding the abundance ratio of Fe to Mg. We suggest that the observed trend reflects the possible cosmic evolution of the Fe/Mg ratio and is consistent with the predictions of a simple model where the abundance ratio variations are driven by the ratio of the rates of SNIa to CCSN.

Throughout this paper, we adopt a cosmology with $[\Omega_m, \Omega_\Lambda, \sigma_8, h] = [0.3, 0.7, 0.8, 0.7]$. Magnitudes are presented in AB units (Oke & Gunn 1983) unless otherwise specified.

2 SAMPLE DEFINITION

In this work, we make use of the JHU-SDSS Metal Absorption Line Catalog (Zhu & Ménard 2013, ; hereafter ZM13) based on the SDSS DR7 release (Abazajian et al. 2009)[1].

This catalog of 35,752 MgII absorption line systems is constructed from 84,533 quasar spectra from SDSS DR7 and covers the redshift range between about 0.4 and 2.2 (determined by the wavelength coverage of the SDSS spectrographs; York et al. 2000). The window function, completeness and purity of the catalog were determined and cross-

[1] http://www.pha.jhu.edu/ gz323/jhusdss

checked using different approaches, including Monte Carlo simulation for the whole sample and redshift path determination for individual quasars (see ZM13 for details). The statistical incidence rate of the Mg II doublet as a function of redshift and strength was also presented in ZM13 and compared with the literature.

The systematic effects in the catalog are also well understood. The primary systematic effects are: (1) the imperfect calibration of the relative spectrophotometry, due to imperfect F-star SED models; (2) the absorption induced by ISM/CGM of the Milky Way at given observer-frame wavelengths, most importantly at 3934Å and 3969Å (due to Ca II), 5891Å and 5897Å (due to Na I), and various diffuse interstellar bands; (3) poor subtraction of the telluric emission lines, which were, on average, under-subtracted in the reduction pipeline; and (4) relatively low completeness at both the short and long wavelength ends due to the reduced throughput at the blue end of the SDSS spectrographs and the poor subtraction of the bright OH lines at the red end. Finally, comparisons of the ZM13 catalog to an independently constructed DR7 catalog find good agreement in the measured equivalent widths in the two catalogs, with the difference in W_{MgII} measurements less than 0.02 Å (Seyffert et al. 2013; Gauthier et al. 2014).

The ZM13 catalog therefore represents a well-understood dataset that spans a large range in redshift; the known systematics have negligible effects on any of the statistics derived here. The spectrophotometric calibration errors are at $\approx 10^{-3}$ level (about an order of magnitude smaller than the photon Poisson noise) and therefore have no effect on the statistics presented here. The absorption by Galactic Ca II can be strong along some lines of sight and does affect the detection efficiency of extragalactic Mg II absorbers below redshift 0.43. We therefore choose not to include the absorbers at $z < 0.43$ in our sample. In addition, we restrict the fits and statisitical analyses to $z > 0.55$ to ensure all detected FeII$\lambda 2600$ lines lie in the region of higher completeness at $\lambda > 4000$Å. The terrestrial lines are known to be under-subtracted and the noise (i.e., flux errors) at corresponding wavelengths were adjusted in accordance in the SDSS reduction pipeline. The Mg II detection pipeline has been fully-tested on cases with poor sky subtraction and shown to perform at the same efficiency as along other sightlines. These tests are discussed in detail in Zhu & Ménard (2013) and Lan et al. (2014). At the red end, we restrict our analyses to $z < 1.90$, which corresponds to MgII detections at roughly $\lambda < 8100$Å.

We extracted all measurements of the MgII $\lambda\lambda 2796.35, 2803.53$, MgI$\lambda 2853$, FeII $\lambda\lambda 2586.00, 2600.73$ absorption lines. The catalog contains a total of 35,752 absorption line systems, >97% of which are "strong" absorbers with $W_{\mathrm{MgII2796}} > 0.3$Å. Since a few of these are only detected marginally, we restricted our analyses to a subset of 35,049 systems with absorption line signal-to-noise ratios of $\mathrm{SNR}_{\mathrm{MgII}} \equiv W_{\mathrm{MgII}}/\sigma_{W_{\mathrm{MgII}}} \geq 3$, where W_{MgII} is the sum of the equivalent widths of the MgII 2796.35 and 2803.53 resonance lines and $\sigma_{W_{\mathrm{MgII}}}$ is the measurement uncertainty; 99.5% of these have $W_{\mathrm{MgII2796}} > 0.3$. No restriction was placed on the strength of the FeII line (hereafter FeII refers to the 2600.73 line). 31,727 of the systems lie at $0.55 \leq z \leq 1.90$ and constitute our primary statistical sample.
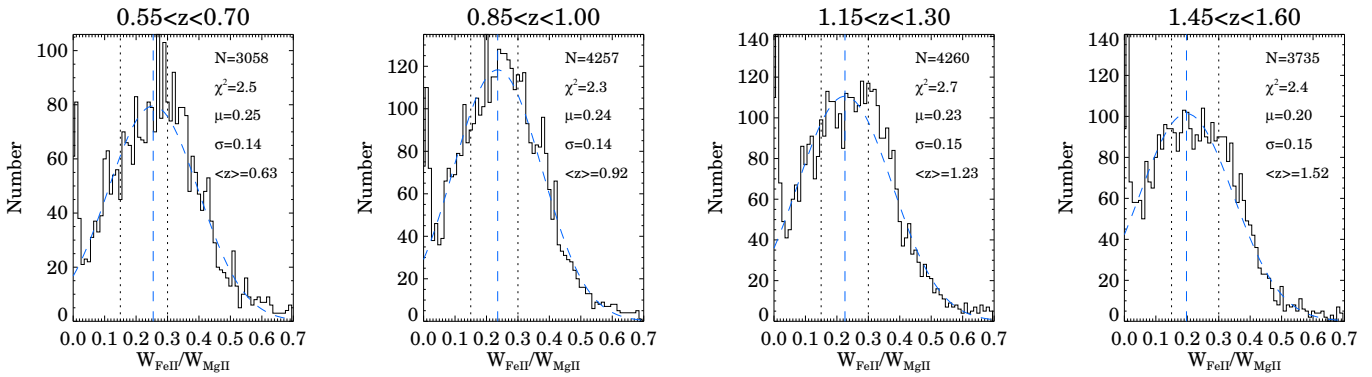
Figure 1. The histograms show sample distributions of the equivalent width ratios in four different redshift bins. The vertical dotted lines at $W_{\rm FeII}/W_{\rm MgII} = 0.15$ and 0.30 are shown as fiducials. The gaussian fits discussed in the text are shown as dashed curves with the peak value shown by the vertical dashed line. The legend in each panel lists the number of absorbers in the redshift bin (N), the χ^2 value of the gaussian fit, the mean (μ) and standard-deviation (σ) of the best-fit gaussian, and the median redshift ($<z>$) of the absorbers within the bin.

3   RESULTS AND ANALYSIS

For each absorber, we defined the ratio $\mathcal{R} \equiv W_{\rm FeII}/W_{\rm MgII}$. The distribution of $\mathcal{R}$ shows a broad distribtion which is roughly gaussian with a weak tail to high values of $\mathcal{R}$. Of the 31,727 absorbers, 4,965 (15.6%) have $\mathcal{R} \le \sigma_{\mathcal{R}}$. The redshift distribution of these sources is similar to the overall distribution of absorbers.

Given the large scatter in the points and the non-detections of FeII, we considered multiple approaches to determining whether there is a trend of $\mathcal{R}$ with redshift and estimating its significance.

3.1   Fits to the $W_{\rm FeII}/W_{\rm MgII}$ Point Distribution

A least-absolute deviation fit to the overall point distribution using 1000 bootstrap samples (with replacement) results in a median slope of $\Delta \mathcal{R}/\Delta z = -0.046 \pm 0.003$. The 95% confidence limits on the slope are [-0.040,-0.052].

Given the significant fraction of FeII non-detections, we also measured the linear regression using the expectation-maximization (EM) technique and Schmitt's binned linear regression method, as implemented in the ASURV package (Lavalley et al. 1992; Isobe et al. 1986). All points with $\mathcal{R} \le \sigma_{\mathcal{R}}$ were treated as upper limits. The EM method resulted in a slope estimate of -0.0406 ± 0.0035. Schmitt's method was used with a redshift binning of $\delta(z) = 0.15$ and $\mathcal{R}$ binning

of $\delta(\mathcal{R}) = 0.05$ and resulted in a slope estimate of -0.034. We investigated different bin sizes, but the results did not change significantly.

Finally, we used the Bayesian approach to linear regression developed by Kelly (2007). This was very CPU-intensive and slow for our sample size, but resulted in a median slope of -0.0304 with a 95% confidence range of $[-0.0343, -0.0252]$.

3.2   Fits to the Shape of the $W_{\rm FeII}/W_{\rm MgII}$ Distribution

We next investigate the redshift evolution in the shape of the distribution of $\mathcal{R} \equiv W_{\rm FeII}/W_{\rm MgII}$. In this approach, non-detections were just placed at their "measured" or edited value; given that the non-detections follow the redshift distribution of the detected sample, any widening of the overall distribution is likely to be similar in all redshift bins.

Following ZM13, we divided the sample into 12 redshift bins defined between the redshifts $z=[0.43,0.55,0.70,0.85,1.00,1.15,...,2.05,2.30]$ and measured the distribution of the ratio $\mathcal{R} \equiv W_{\rm FeII}/W_{\rm MgII}$ in each bin. We modeled the distribution in each redshift bin as a gaussian (fit using a non-linear least squares method) and found the best fit value for the gaussian mean. We also computed the median value of the distribution within each bin. Fig. 1 shows the distributions and the fits in a few sample redshift bins. We then performed linear fits (using least absolute deviation and least squares techniques) to the median and mean values to measure the variation of $\mathcal{R}$ with redshift.

In order to understand the uncertainty that may be inherent in this analysis due to the effects of a complex and censored sample, we carried out a bootstrap analysis by selecting samples using replacement from the data in each redshift bin. For each bootstrap sample, we carried out the same analyses (i.e., measuring medians, fitting gaussians, and fitting the median and means as a linear function of redshift).

The results for the primary sample (i.e., 31,727 $W_{\rm MgII}/\sigma_{W_{\rm MgII}} \ge 3$ absorbers) are shown in Figure 2. The distribution of points is shown as a greyscale with the median and quartiles represented as thin black lines. The best

4   *Dey et al.*

fit peak and median values in each redshift bin are shown as
large filled triangles and circles, respectively, along with the
uncertainties derived in the bootstrap analyses. The peak
and median values of the $\mathcal{R}$ ratio distribution trend to lower
values with increasing redshift. The same behavior is re-
flected in the variation of the quartiles with redshift. A lin-
ear fit to the peak values of the gaussian distribution within
the redshift range $0.55 \leq z \leq 1.9$ (i.e., using redshift bins
with >900 absorbers) results in $\mathcal{R} \propto (-0.049 \pm 0.006)z$ with
95% confidence limits of $[-0.055, -0.036]$; a fit to the median
values results in a similar slope of (-0.045 ± 0.005).

The observed trend is not due to the censor-
ship of the data. For our primary sample we used
the least censored subset. However, we also investigated
subsamples selected with a range of signal-to-noise ra-
tios $\mathrm{SNR_{FeIIorMgII}} \geq [0, 1, 2, 3, 5, 7, 10]$ and found significant
trends (with $\mathcal{R}$ decreasing with increasing redshift in all
cases) and with slopes (derived for fits to the median val-
ues) ranging from -0.030 to -0.056, with a median de-
rived slope value of ≈ -0.045. The steepest (shallowest)
slope values are found for the $\mathrm{SNR_{MgII}} \geq 7$ and $\mathrm{SNR_{FeII}} \geq 0$
($\mathrm{SNR_{MgII}} \geq 10$ and $\mathrm{SNR_{FeII}} \geq 10$) sample containing 20,813
(2,962) absorbers (see Table 1).

While higher SNR thresholds tend to select higher
equivalent width lines, the correspondence between the two
quantities is complicated and the equivalent width distri-
bution at a given signal-to-noise threshold varies in a com-
plicated way with wavelength. Hence, in order to further
investigate whether the trend is dominated (or damped) by
stronger absorbers, we investigated subsamples with a range
of W_{MgII} and W_{FeII} equivalent width cutoffs, selecting sam-
ples with equivalent width cuts > $[0, 0.5, 1.0, 1.5, 2.0]$ in either
line. The derived slopes do not vary in a monotonic way with
the equivalent width cuts, and there is no evidence from the
current dataset that a subset of stronger or weaker absorbers
are dominating the trend signal (see also Fig. 3 right panel).

The trend of $\mathcal{R}$ with redshift appears to be primarily
driven by an evolution in the FeII equivalent width. Fit-
ting the medians of the distributions of the MgII and FeII
equivalent widths as a function of redshift results in mea-
sured slopes of -0.06 ± 0.05 for W_{MgII} vs. z and -0.20 ± 0.02
for W_{FeII} vs. z. The non-evolution in the slope of W_{MgII}
observed in our data is consistent with the results from
previous high-spectral-resolution studies (Mshar et al. 2007;
Churchill et al. 2003).

3.3 Are Selection Effects Responsible for the Trend?

We have established that the absorption line systems
listed in the JHU-SDSS catalog exhibit a trend where the
$W_{\mathrm{FeII}}/W_{\mathrm{MgII}}$ decreases with redshift. Although the catalog
is constructed from the spectra of QSOs observed uniformly
with the SDSS spectrographs, it is important to consider
whether the observed trend could be the result of observa-
tional selection effects.

As an initial test, we investigated whether the line ratios
MgII $\lambda2796$/MgII $\lambda2803$ and FeII $\lambda2586$/FeII $\lambda2600$ in our
sample show significant variation with redshift; they do not,
and fits (to SNR$\geq$3 samples) result in slopes of -0.01 ± 0.13
and -0.03 ± 0.01 respectively (see also the left two pan-
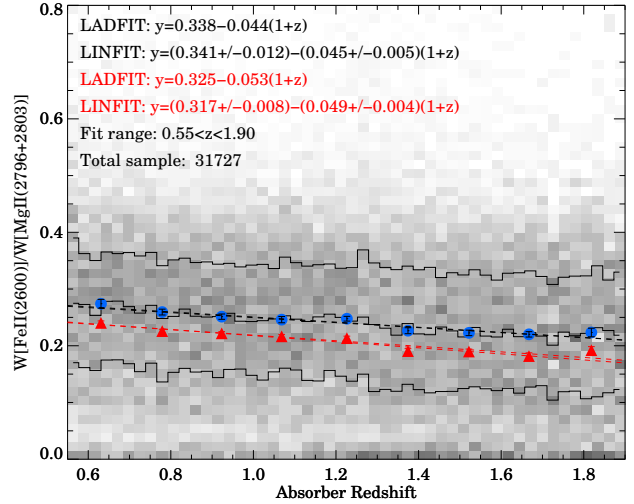els of Fig. 3). In addition, the MgI$\lambda2853$/MgII equiva-

Figure 2. Distribution of the ratio of the FeII $\lambda2600$ to MgII
$\lambda\lambda2796,2803$ equivalent widths as a function of redshift. The
greyscale show the distribution of all absorption line systems from
the JHU-SDSS Absorption Line Catalog (Zhu & Ménard 2013)
with > 3σ W_{MgII} measurements. The thin black lines show the
median and quartiles of the distribution. The solid blue circles
show the median values in different redshift bins; the solid pink
triangles show the peak of gaussian fits to the ratio distribution
(see text). The dashed lines show linear fits to the two sets of
solid points. The grey hashed region denotes the range of slopes
resulting from the Monte Carlo simulations of the null hypothesis
(i.e., intrinsic $\mathcal{R}$ constant with redshift) described in the text. A
small fraction (1.4%) of the absorbers have ratios larger than the
y-limit shown. We include them in our analyses, but they have
no effect on the results.

width ratio does not vary significantly with redshift (slope of
0.02 ± 0.01). Changing the subsamples by varying the signal-
to-noise ratio cutoff does not change these results signifi-
cantly, although in the case of the FeII $\lambda2586$/FeII $\lambda2600$
ratio, higher SNR cuts result in a slightly more significant
detection of a trend (e.g., for SNR>5, FeII $\lambda2586$/FeII $\lambda2600$
vs. redshift has a slope of -0.045 ± 0.010). While the wave-
length separation between these various features is smaller
than that between the MgII and FeII features, there does not
appear to be any systematic effect introduced by the fact
that the lines are measured in different parts of the spec-
trum. The division in spectral coverage between the blue
and red spectrographs at $\lambda \sim 5800$Å does result in a lower
detection efficiency of absorption lines at these wavelengths
and results in a slightly higher median equivalent width for
the $z \approx 1.2$ bin; however, there is no obvious feature in the
distribution of the line ratios and this bin does not affect
the determination of the overall trend.

In order to determine whether the complicated selec-
tion function for absorption line detection could be respon-
sible for the trend, we used the measured selection function
from ZM13 to create 1000 simulated datasets as follows.
We simulated a large number of MgII absorption lines (dis-
tributed randomly in redshift within each redshift bin) using
the best-fit intrinsic exponential distribution of rest equiva-
lent width computed by ZM13 (see equation 3 and table 1
in ZM13). For each MgII absorber, the $W_{\mathrm{MgII2796}}/W_{\mathrm{MgII2803}}$

© 0000 RAS, MNRAS **000**, 000–000

SNR(MgII)	SNR(FeII)						
	≥0	≥1	≥2	≥3	≥5	≥7	≥10
≥0	-0.0430±0.0048	-0.0506±0.0046	-0.0590±0.0044	-0.0522±0.0060	-0.0417±0.0046	-0.0355±0.0061	-0.0325±0.0069
	-0.0468±0.0044	-0.0678±0.0034	-0.0569±0.0030	-0.0522±0.0027	-0.0432±0.0030	-0.0372±0.0033	-0.0339±0.0043
	32167	27042	20487	14873	8687	5483	3044
≥1	-0.0428±0.0050	-0.0505±0.0047	-0.0586±0.0044	-0.0524±0.0056	-0.0417±0.0046	-0.0353±0.0062	-0.0331±0.0071
	-0.0470±0.0043	-0.0674±0.0034	-0.0570±0.0030	-0.0525±0.0027	-0.0431±0.0030	-0.0373±0.0034	-0.0339±0.0042
	32157	27034	20483	14869	8686	5483	3044
≥2	-0.0432±0.0048	-0.0508±0.0047	-0.0590±0.0045	-0.0527±0.0056	-0.0420±0.0047	-0.0351±0.0063	-0.0325±0.0066
	-0.0468±0.0042	-0.0673±0.0035	-0.0569±0.0028	-0.0525±0.0028	-0.0434±0.0031	-0.0372±0.0034	-0.0338±0.0041
	32137	27021	20474	14866	8686	5483	3044
≥3	**-0.0445±0.0049**	-0.0496±0.0046	-0.0583±0.0042	-0.0516±0.0053	-0.0417±0.0047	-0.0351±0.0061	-0.0319±0.0068
	-0.0487±0.0045	-0.0667±0.0034	-0.0568±0.0030	-0.0524±0.0028	-0.0432±0.0030	-0.0370±0.0034	-0.0336±0.0040
	31727	26864	20447	14851	8679	5478	3043
≥5	-0.0543±0.0051	-0.0478±0.0045	-0.0521±0.0047	-0.0503±0.0056	-0.0410±0.0046	-0.0333±0.0061	-0.0315±0.0069
	-0.0582±0.0042	-0.0634±0.0036	-0.0525±0.0028	-0.0520±0.0028	-0.0430±0.0030	-0.0370±0.0034	-0.0336±0.0043
	27602	24397	19655	14663	8647	5457	3035
≥7	-0.0578±0.0043	-0.0487±0.0054	-0.0431±0.0045	-0.0481±0.0048	-0.0416±0.0045	-0.0337±0.0059	-0.0308±0.0069
	-0.0608±0.0037	-0.0599±0.0034	-0.0473±0.0030	-0.0474±0.0026	-0.0438±0.0029	-0.0372±0.0035	-0.0340±0.0042
	20813	19357	16896	13619	8495	5396	3008
≥10	-0.0563±0.0078	-0.0499±0.0064	-0.0459±0.0048	-0.0441±0.0042	-0.0427±0.0051	-0.0364±0.0054	-0.0305±0.0067
	-0.0610±0.0039	-0.0601±0.0039	-0.0491±0.0033	-0.0455±0.0029	-0.0448±0.0030	-0.0410±0.0032	-0.0353±0.0043
	13483	13028	12234	10879	7859	5222	2962

Table 1. Trend slopes for subsamples defined by censoring the data by the signal-to-noise ratio in W_{FeII} and W_{MgII}. For each pair of signal-to-noise ratio cuts, the top entry is the median slope and 1σ error (determined using bootstrap resampling) determined by fitting (using least absolute deviation) the median values in each redshift bin; the middle entry is the median and 1σ error for the slope determined by a linear least squares fit to the mean of the gaussian model for the distribution; and the bottom entry is the total number of absorbers in the censored sample. The primary sample used in this paper is the one listed in bold face for SNR(Mg)$\geq$3 and SNR(Fe)$\geq$0.

doublet ratio was drawn from a lognormal model based on a fit to the observed distribution of the ratio in the JHU-SDSS dataset. Then, for each MgII absorber, an FeII absorption line was drawn randomly from a normal distribution of $\mathcal{R}$ with a mean of 0.233 and σ=0.143. In order to test whether the selection would generate a systematic bias, the $\mathcal{R}$ distribution was assumed to be constant with redshift. Equivalent width uncertainties for the MgII and FeII lines were assigned randomly, drawn from model fits to the actual fractional error distributions in these two lines. In each case, we constructed the two-dimensional distribution of σ_W/W versus W and modeled the surface as a lognormal in σ_W/W and a polynomial in W. We then "observed" this set of intrinsic MgII+FeII absorbers using the equivalent width selection function for the JHU-SDSS catalog (ZM13). We selected absorbers and fit each of the 1000 such datasets in the same manner in which we fit the observed catalog and derived slope measurements for any gradient in $W_{\mathrm{FeII}}/W_{\mathrm{MgII}}$ ratio with redshift. Since there was no evolution assumed in the data, any resulting slope is purely due to selection effects (i.e., completeness as a function of equivalent width and observed wavelength) and the variation in the intrinsic distribution of W_{MgII} with redshift.

We do not detect the observed slope in the simulated $\mathcal{R}$ distribution with a high degree of reliability. The 1000 trials resulted in a normal distribution of slopes with a small negative bias (median recovered slope = -0.0148; standard deviation of 0.0033); the 95% (99%) confidence limits on the slope are $[-0.021, -0.008]$ ($[-0.023, -0.0062]$) and none of the 1000 trials resulted in slope determinations ≤ -0.0245. We therefore conclude that the observed trend is not the result of selection effects.

4 DISCUSSION

Our results show that the ratio of the equivalent widths of FeII to MgII absorption lines along the lines of sight to QSOs decreases with redshift. The trend survives a range of signal-to-noise ratio or equivalent width cuts and does not appear to be due to selection effects within the JHU-SDSS ZM13 dataset. In this section, we discuss possible physical origins for the equivalent width ratio evolution.

The strength of an isolated absorption line as measured by its equivalent width is related to its abundance in the gas phase and the velocity spread of the gas (Menzel 1936; Baker 1936; Aller 1942). It is tempting to interpret the $W_{\mathrm{FeII}}/W_{\mathrm{MgII}}$ ratio in terms of the Fe/Mg abundance ratio. However, in order to interpret the observed equivalent widths in terms of physical quantities associated with the

absorbing clouds, we need to consider the effects of (i) saturation, (ii) kinematics, (iii) ionization, and (iv) depletion. We consider each of these in turn.

(i) Line Saturation: The W_{MgII} distribution for the SNR$\geq$3 sample is a lognormal which peaks at ≈ 2Å, implying that the individual doublet lines have typical equivalent widths >1Å and lie in the logarithmic (i.e., "saturated") part of the curve of growth. It is therefore not obvious that we can interpret any observed trend with redshift as resulting from a trend in the abundance ratio of Mg to Fe without first understanding the effects of line saturation.

In order to investigate the effects of saturation on the observed ratio, we computed the curves of growth for MgII and FeII for two different values of the Doppler parameter, b_D=10 km s^{-1} and 50 km s^{-1}. For each case, we computed the expected $\mathcal{R}$ values that result from a wide range in MgII column density $12 \leq \log(N_{\mathrm{MgII}}) \leq 17.9$ and [Mg/Fe] varying between 1 and 10 times the solar value. For a given b_D, even strongly saturated lines result in the equivalent width ratio $\mathcal{R}$ depending on the [Mg/Fe] abundance ratio. Hence, even if the observed absorption lines are single and saturated, they only dampen, but not erase, an intrinsic variation of the abundance ratio. Most MgII absorption systems with $W_{\mathrm{MgII}} > 0.3$Å are multiple systems (e.g., Churchill et al. 2003), and this complicates the simple picture described here. Fully modeling the result of saturation and multiplicity is beyond the scope of this paper, but instead we look to the data for clues to whether saturation effects are responsible for the observed trends.

Fig. 3 shows the effect of saturation on three pairs of equivalent width ratios in our observational dataset. The $W_{\mathrm{MgII2796}}/W_{\mathrm{MgII2803}}$ and $W_{\mathrm{FeII2586}}/W_{\mathrm{FeII2600}}$ ratios (shown in the first two panels) asymptote toward the saturation value with increasing W_{MgII}. However, neither of these ratios shows any evolution with redshift. In contrast, the $W_{\mathrm{FeII}}/W_{\mathrm{MgII}}$ ratio clearly evolves, with the median line ratio decreasing with increasing redshift in *all* W_{MgII} bins. Fig. 3 also shows that the higher equivalent width bins also exhibit the evolution with redshift, albeit at lower strength than the lower equivalent width (and less saturated) bins. This is consistent with our expectation that saturation effects will tend to weaken the relationship between $\mathcal{R}$ and the intrinsic FeII/MgII abundance ratio of the absorbers, and then that these effects are likely only to dampen (rather than induce) a potential trend in $\mathcal{R}$ with redshift.

(ii) Multiplicity & Kinematics:

If the observed absorption lines are instead the result of blends of multiple unresolved (lower equivalent width) lines, then the individual lines might arise in lower column density clouds and are therefore presumably less saturated. The real situation is likely to be more complicated, with lines forming in clouds with varying kinematic properties.

High-resolution studies have demonstrated that MgII lines are often made up of a number of components, typically between 2 and 10, with the number of components increasing with W_{MgII} (Churchill et al. 2003). However, they also find that the MgII and FeII absorption lines show similar Doppler parameters and correlated column densities and the distribution of $N(\mathrm{FeII})/N(\mathrm{MgII})$ column ratios does not depend strongly on velocity spread (Churchill et al. 2003), nor does the kinematic spread show any evidence for significant evolution with redshift (Mshar et al. 2007; Churchill et al.

2000). Hence, assuming the FeII and MgII absorption lines are equally sensitive to the variations in the clouds as they evolve, the evolution of the ratio $W_{\mathrm{FeII}}/W_{\mathrm{MgII}}$ for individual absorption systems should change monotonically with the abundance ratio $N_{\mathrm{FeII}}/N_{\mathrm{MgII}}$, although the magnitude of the change may be dampened by saturation effects. If, for some reason, the velocity structure or Doppler parameter for these two species differs, due to e.g., differences in ionization structure or incomplete mixing of metal species, this monotonic relation can break down. For example, incomplete metal mixing could arise in a delayed Fe-enrichment scenario: if the kinematic spread of Fe-rich material is narrower than that of α-enriched gas, this could give rise to a suppressed $W_{\mathrm{FeII}}/W_{\mathrm{MgII}}$ ratio without it reflecting a true dearth of Fe atoms. However, even if this somewhat contrived scenario were realized, it would still point to an evolution in the sources of CGM enrichment. While it may be possible to create a trend in $\mathcal{R}$ with redshift as a result of an evolving b_D, there is no obvious reason why the Doppler parameter would evolve with redshift for just one species. Better spectroscopic data (higher spectral resolution, and on more species and ionization states) on much larger samples than currently exist can help explore this issue further.

(iii) Ionization Correction: The first two ionization potentials for Mg and Fe are very similar: for MgI$\rightarrow$MgII and FeI$\rightarrow$FeII, they are 7.646 eV and 7.902eV respectively; the second ionization potentials (i.e., MgII$\rightarrow$MgIII and FeII$\rightarrow$FeIII) are 15.0357 eV and 16.1878 eV respectively (Morton 2003; Kramida et al. 2013). The ratio of the ionic abundances of the two elements, $N_{\mathrm{MgII}}/N_{\mathrm{FeII}}$, is determined by the shape (at these energies) of the spectrum of the ionizing metagalactic radiation, which does not vary significantly over the redshift range considered here. Using the Haardt & Madau (2012) model for the UV metagalactic flux as a function of redshift, we find that the ratio of the emissivity at the Mg and Fe 1st ionization potentials varies by less than 4% for $0.4 < z < 2.0$; the emissivity ratio at the wavelengths of the 2nd ionization potential varies by less than 2%.

The bulk of the absorbers (>96%) in the JHU-SDSS Metal Absorption Line Catalog have $W_{\mathrm{MgII2796}} > 0.5$Å. These absorbers therefore correspond to regions with hydrogen column densities of $\log(N_{\mathrm{HI}}) > 19.4$ (if the Doppler parameter is 10 km s^{-1}; Ménard & Chelouche 2009). Giavalisco et al. (2011) calculate the variation of the N(MgII)/N(FeII) ratio with ionization parameter for the Haardt & Madau (1996) metagalactic radiation field. They find that for hydrogen column densities $\log(N_{\mathrm{HI}}/\mathrm{cm}^{-2}) > 19$, the N(MgII)/N(FeII) ratio (and hence its inverse) is essentially constant over a wide range of ionization parameter (see also Crighton et al. 2015).

It is therefore unlikely that differences in ionization could drive the observed trend.

(iv) Depletion: MgII absorption line systems are known to contain dust, exhibiting dust-to-gas ratios comparable to that observed for normal galaxies (Ménard & Fukugita 2012). Since both Mg and Fe can be depleted onto dust grains, it is necessary to understand whether differing depletion rates for the two elements as a function of redshift can result in the trend observed in their equivalent width ratios.
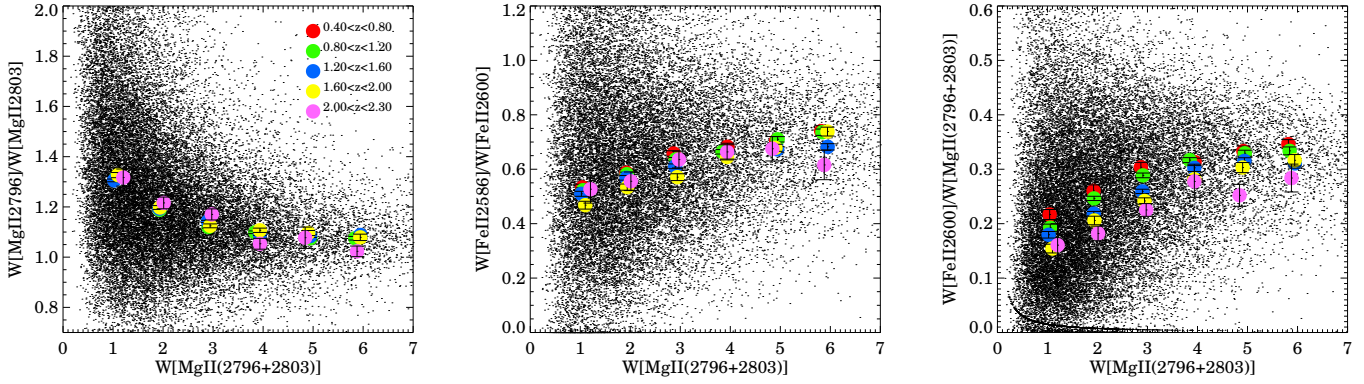
Based on studies of the interstellar medium in our

Figure 3. The impact of line saturation, shown as the variation of $W_{\mathrm{MgII2796}}/W_{2803}$ (Left panel), $W_{\mathrm{FeII2586}}/W_{\mathrm{Fe2600}}$ (Middle panel), and $W_{\mathrm{FeII}}/W_{\mathrm{MgII}}$ (Right panel) with the MgII equivalent width. The small points show the distributions for the $\geq 3\sigma$ sample described in the text and the large coloured circles show the median values of the distributions in the redshift bins shown in the legend. The left two panels show that the ratio asymptotes to a constant value with increasing W_{MgII}, suggesting that the lines are becoming saturated, but that the behavior is the same at all redshifts. In contrast, the $W_{\mathrm{FeII}}/W_{\mathrm{MgII}}$ (Right panel) shows a systematic evolution with redshift in all W_{MgII} bins.

Galaxy, the depletion rate for Fe is approximately $2-7$ times larger than that for Mg (e.g., Savage & Sembach 1996), i.e., Fe is depleted from the gas phase at a higher rate than is Mg. Using the tabulated model of Jenkins (2009) for the dependence of the Mg and Fe gas phase abundance on the line-of-sight depletion strength F_*, we find that the column density ratio $\log(N_{\mathrm{Mg}}/N_{\mathrm{Fe}})$ varies as $(0.29\pm0.06)F_*$, i.e., the gas-phase column density ratio increases with increasing depletion and dustier absorbing clouds (which would presumably be more depleted in Mg and Fe) would exhibit higher values of $\log(N_{\mathrm{Mg}}/N_{\mathrm{Fe}})$. Hence, the only way to reproduce a trend where the $W_{\mathrm{FeII}}/W_{\mathrm{MgII}}$ ratio decreases with redshift through purely dust depletion effects is to have higher redshift absorbers be dustier (and more depleted) than lower redshift absorbers, an unlikely scenario.

In contrast, we expect Fe and dust content to increase as the Universe ages and that Fe is likely to be fractionally more depleted onto dust at lower redshift. Hence, any detection of an increase (to lower redshift) in the observed gas-phase Fe/Mg abundance ratio is likely to reflect a stronger intrinsic increase in the abundance ratio. In other words, a measurement of the gas-phase Fe/Mg ratio would underestimate the true Fe/Mg, and the factor by which it is underestimated would be larger at low redshift than at high redshift. This goes in the sense, therefore, of making the observed relation imply a stronger underlying variation. It is therefore unlikely that depletion effects could explain away the observed trend.

4.1   *A Simple Physical Model*

In contrast to various possible (and somewhat contrived) explanations discussed above, the expected variation of the rates of SNIa and CCSN should naturally produce the observed variation in $\mathcal{R}$ and we therefore consider this next.

We model the average universal Fe/Mg abundance ratio as resulting from the supernovae formed at each epoch as a result of the cosmic star formation rate history.[2] We assume that the rate of core collapse supernovae follows the cosmic star formation rate density, i.e., $r_{\mathrm{CCSN}} \propto \psi(z)$ (e.g., Madau & Dickinson 2014). Since CCSN progenitors are massive ($M > 8M_\odot$) stars, the rate of CCSN is closely tied to the cosmic star-formation rate density in the Universe, i.e.,

$$R_{\mathrm{CC}}(z) = 0.0068\psi(z)\,\mathrm{yr}^{-1}\,\mathrm{Mpc}^{-3}, \qquad (1)$$

where $\psi(z)$ is the cosmic star formation rate density (in units of $\mathrm{M}_\odot\,\mathrm{yr}^{-1}\,\mathrm{Mpc}^{-3}$; Madau & Dickinson 2014). $R_{\mathrm{CC}}(z)$ assumes a Salpeter initial mass function with $8 < M < 40\,\mathrm{M}_\odot$ (Madau & Dickinson 2014). In contrast, SNIa rates exhibit a "delay time distribution" (DTD) relative to the time since star formation (e.g., Totani et al. 2008; Maoz & Mannucci 2012; Maoz et al. 2012; Claeys et al. 2014). Since there is much debate about the exact form of this distribution, here we assume the simple power-law form suggested by Maoz & Mannucci (2012):

$$R_{\mathrm{Ia}}(t) = \int_0^t \psi(t-\tau)\mathrm{DTD}(\tau)\mathrm{d}\tau\,\mathrm{yr}^{-1}\,\mathrm{Mpc}^{-3}, \qquad (2)$$

where $\mathrm{DTD}(\tau) = 4 \times 10^{-13}(\tau/1\mathrm{Gyr})\,\mathrm{yr}^{-1}\mathrm{M}_\odot^{-1}$.

We compute the evolving mass density of each element as the sum of the SN yields:

$$M_X = Y_X^{\mathrm{SNIa}} \int_0^t R_{\mathrm{SNIa}}(t)dt + Y_X^{\mathrm{CCSN}} \int_0^t R_{\mathrm{CCSN}}(t)dt, \quad (3)$$

where Y_X^{S} is the average mass yield for metal X (in $\mathrm{M}_\odot$) for a SN of type S. The number density of element X is M_X/A_X, where A_X is the relative atomic mass of element X. The SN yields are very uncertain: based on a review of the literature, Wiersma et al. (2009) conclude that calculated nucleosynthetic yields from SNe vary by factors of ≈ 2. Here,

---

[2] We ignore the contribution of AGB stars here because (a) supernovae dominate the metal enrichment, and (b) we are considering absorption line systems which likely are clouds at large distances from the galaxy nucleus or disk, where the enrichment is probably due to energetic SN ejecta.
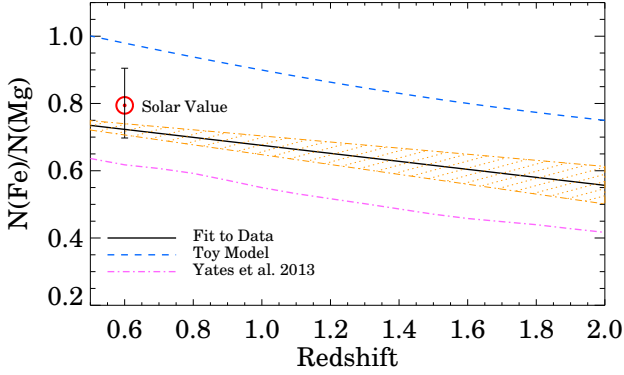
Figure 4. The blue dashed line shows the variation of Fe/Mg abundance ratio with redshift predicted by the simple model described in the text, based on a CCSN rate tied to the Madau & Dickinson (2014) star-formation rate density and the Maoz & Mannucci (2012) power-law delay time distribution for the SNIa rate. The dot-dashed purple line shows the variation with redshift of the Fe/Mg ratio computed by Yates et al. (2013) for a model Milky Way - type galaxy. The red circle with the error bar represents the solar abundance ratio. The solid line and the hashed region surrounding it show, respectively, the observed variation in the equivalent width ratio $\mathcal{R}$ and the 99.5% confidence limits on the slope. We have normalized the fit to match the solar value at $z = 0$, under the assumption that the abundances are linearly proportional to the equivalent widths.

we assume that the typical SNIa produces $8.6 \times 10^{-3} M_\odot$ of Mg and $0.74 M_\odot$ of Fe, and that the typical CCSN produces 0.12 $M_\odot$ of Mg and 0.09 $M_\odot$ of Fe (Nomoto et al. 1997). Choosing a single number for the average yields is a simplification, but our aim here is to explore whether the overall variation observed in the $W_{\mathrm{FeII}}/W_{\mathrm{MgII}}$ ratio can be explained by just the simple evolution of the SN rates.

The results are shown in Fig. 4. The solar abundance ratio of $(N_{\mathrm{Fe}}/N_{\mathrm{Mg}})_\odot = 0.794^{+0.111}_{-0.097}$ is also shown (based on the Mg and Fe photospheric abundances of 7.60±0.04 and 7.50±0.04 respectively; Asplund et al. 2009). This simple model over-predicts the observed SNIa rates by a factor of 2 and over-predicts the solar photospheric abundance ratio of Fe/Mg at redshift $z = 0$ by $\approx 40\%$. This is not surprising given the large uncertainties in the yields and our other assumptions (e.g., ignoring the contribution from AGB stars, uncertainties/variations in the IMF, DTD, SFRD, and the large scatter in the data).[3]

Recently, Yates et al. (2013) modeled the metal enrichment in a galaxy resulting from AGB stars and SNe, investigating different assumptions for SN yields and SNIa DTDs. They find that the observed local mass-metallicity relationships and the [O/Fe] abundance in the Milky Way can be reproduced by models in which the SNIa DTD is a power-law and the light α elements are expelled in galactic winds. The redshift variation of the Fe/Mg ratio computed by Yates et al. (2013) for a model Milky Way - type galaxy using a power-law DTD is also shown in Fig. 4; rather re-

markably, its slope matches the evolution in $\mathcal{R}$ observed in the JHU-SDSS dataset. This lends further, though still circumstantial, support that the observed evolution can be explained as the result of the increasing dominance of SNIa yields changing the mean composition of the outflowing gas responsible for the absorption line systems over time.

The comparisons of the models to the slopes measured in the data are only meant to be illustrative and not discriminatory. The scatter in the slope measurement is large and the models are only notional at this stage. Nevertheless it is instructive that the measured variation shows slopes comparable to those predicted by models where all the evolution in the abundance ratios is the result of star formation in galaxies and enriched material ejected into their gaseos halos. The large scatter in the data may reflect the diversity of star formation histories, impact parameters of QSO lines of sight through halos, and inhomogeneities in the halo gas.

Individual absorbers at any given redshift show significant scatter and the trend (of $\mathcal{R}$ with z) reported here is subtle; it was only possible to measure the trend using the very large catalog of absorbers resulting from the SDSS QSO spectra. It is therefore not surprising that previous high-resolution studies (e.g., Churchill et al. 2003; Mshar et al. 2007; Narayanan et al. 2008; Rodríguez Hidalgo et al. 2012) did not see the trend of $\mathcal{R}$ with redshift in the small samples (< 100 absorbers) studied (however, please see Srianand (1996)'s analysis of the Steidel & Sargent (1992) dataset, where a possible trend of decreasing $W_{\mathrm{FeII}\lambda2382}/W_{\mathrm{MgII}}$ is reported). In a VLT/UVES high-resolution study of 100 weak (i.e., $W_{\mathrm{MgII}2796} < 0.3$Å) MgII absorbers, Narayanan et al. (2008) found that clouds with high $W_{\mathrm{FeII}}/W_{\mathrm{MgII}}$ disappear from their sample at high redshift ($z > 1.2$). In a complementary study of 81 strong absorbers identified in the same dataset, Rodríguez Hidalgo et al. (2012) found that the $W_{\mathrm{FeII}}/W_{\mathrm{MgII}}$ ratio for $W_{\mathrm{MgII}2796} > 1$Å absorbers is typically high and exhibits some evolution with redshift; weaker absorbers (0.3Å$< W_{\mathrm{MgII}2796} < 1$Å) instead showed a wider range and scatter in the $W_{\mathrm{FeII}}/W_{\mathrm{MgII}}$ ratio with no obvious trend. The authors interpret this as primarily due to kinematics: high-redshift absorbers with $W_{\mathrm{MgII}2796} > 1$Å tend to be formed in regions with more kinematic spread (and the FeII and MgII lines are less saturated) than their low-redshift counterparts. They also consider the effects of ionization and α-enhancement, but conclude that they cannot discriminate between these effects.

The SDSS spectra have insufficient resolution to explore this issue adequately (York et al. 2000). However, splitting the sample into two equivalent width bins — 0.3Å$\leq$ $W_{\mathrm{MgII}2796}$ $<$ 1Å and $W_{\mathrm{MgII}2796}$ $\geq$ 1Å following Rodríguez Hidalgo et al. (2012) — we find that both subsets show evolution (with slopes and 95% confidence ranges of -0.0502, $[-0.0591, -0.0422]$ and -0.0434, $[-0.0516, -0.0344]$ respectively). There is also evidence that the $\mathcal{R}$ values show a much broader distribution for the 0.3Å$\leq W_{\mathrm{MgII}2796} < 1$Å subset than for the $W_{\mathrm{MgII}2796} \geq 1$Å subset. It is not obvious from the large SDSS dataset, therefore, whether splitting the data by equivalent width is justified or if the absorber population should be treated as a continuum, reflecting a range of gas physical conditions in the halos of galaxies.

Given the various caveats already described in using low-resolution data, it will be necessary to obtain high reso-

---

[3] Correcting the R_{SNIa} rate by a factor of 0.6 can result in both a better fit to the observed rates and the solar abundance ratio.

lution spectroscopic observations of a sufficiently large sample (∼1000s) of absorbers to properly disentangle the effects of saturation, kinematics and abundance. A more detailed investigation of the scatter in the equivalent width and ratio distributions compared to the results from numerical simulations will help us further understand the range of physical conditions in galaxy halos.

5 CONCLUSION

We have investigated the equivalent width ratio $W_{\mathrm{MgII}}/W_{\mathrm{FeII}}$ for a large sample of MgII absorption line systems from the JHU-SDSS Metal Absorption Line Catalog of Zhu & Ménard (2013) and discovered that the ratio shows a trend with redshift. This trend does not appear to be the result of data artifacts or selection effects in the catalog. Several reasons may exist for the observed evolution. However, a simple model shows that the trend is naturally explained by the evolving Fe/Mg abundance ratio that results from the changing relative rates of Type Ia and core-collapse SNe. Star-formation (and hence supernovae production) is primarily located in galactic disks, whereas the absorption lines under investigation here form in circumgalactic clouds in galaxy halos at large galactocentric distances. Hence, if the equivalent width ratio reflects abundance variations in the CGM clouds, and if the enrichment by supernovae is indeed the primary cause for the CGM metallicity variations, then outflows must be efficient in transporting metals out of star-forming disks to large galactocentric radii.

Future spectroscopic surveys with the next generation of highly multiplexed multi-object spectrographs (e.g., DESI on the Mayall telescope[4], PFS on Subaru[5], and 4MOST on VISTA[6]) will result in larger samples of absorption line systems and the ability to explore the chemical evolution of the Universe in greater detail. Higher signal-to-noise ratio and higher resolution spectroscopy of large samples spanning a large redshift range can confirm whether the trend observed in the Fe/Mg ratio is observed in other α-element lines and explore whether the changes are due to the chemical enrichment history of the Universe (as suggested here) or if evolution in the cloud properties (e.g., ionization, kinematics, Doppler parameter, substructure, etc.) is instead responsible for the trend. Detailed comparisons between the data and state-of-the-art cosmological simulations (e.g., Vogelsberger et al. 2014) will be critical to this effort.

REFERENCES

Abazajian, K. N., Adelman-McCarthy, J. K., Agüeros, M. A., et al. 2009, ApJS, 182, 543

Aller, L. H. 1942, ApJ, 96, 321

Asplund, M., Grevesse, N., Sauval, A. J., & Scott, P. 2009, ARA&A, 47, 481

Bahcall, J. N., & Spitzer, L., Jr. 1969, ApJ, 156, L63

Baker, J. G. 1936, ApJ, 84, 474

Bergeron, J., & Boissé, P. 1991, A&A, 243, 344

Bordoloi, R., Lilly, S. J., Knobel, C., et al. 2011, ApJ, 743, 10

Churchill, C. W., Mellon, R. R., Charlton, J. C., et al. 2000, ApJ, 543, 577

Churchill, C. W., Vogt, S. S., & Charlton, J. C. 2003, AJ, 125, 98

Claeys, J. S. W., Pols, O. R., Izzard, R. G., Vink, J., & Verbunt, F. W. M. 2014, A&A, 563, A83

Crighton, N. H. M., Hennawi, J. F., Simcoe, R. A., et al. 2015, MNRAS, 446, 18

Dalla Vecchia, C., & Schaye, J. 2008, MNRAS, 387, 1431

Davé, R., Finlator, K., & Oppenheimer, B. D. 2011, MNRAS, 416, 1354

Erb, D. K., Quider, A. M., Henry, A. L., & Martin, C. L. 2012, ApJ, 759, 26

Finlator, K., & Davé, R. 2008, MNRAS, 385, 2181

Gauthier, J.-R., Chen, H.-W., Cooksey, K. L., et al. 2014, MNRAS, 439, 342

Giavalisco, M., Vanzella, E., Salimbeni, S., et al. 2011, ApJ, 743, 95

Haardt, F., & Madau, P. 1996, ApJ, 461, 20

Haardt, F., & Madau, P. 2012, ApJ, 746, 125

Hartigan, P., Morse, J. A., Tumlinson, J., Raymond, J., & Heathcote, S. 1999, ApJ, 512, 901

Isobe, T., Feigelson, E. D., & Nelson, P. I. 1986, ApJ, 306, 490

Jenkins, E. B. 2009, ApJ, 700, 1299

[4] http://desi.lbl.gov/
[5] http://pfs.ipmu.jp/factsheet/
[6] http://www.aip.de/en/research/research-area-ea/research-groups-and-projects/4most

Kelly, B. C. 2007, ApJ, 665, 1489

Kornei, K. A., Shapley, A. E., Martin, C. L., et al. 2012, ApJ, 758, 135

Kramida, A., Ralchenko, Yu., Reader, J., and NIST ASD Team (2013). NIST Atomic Spectra Database (ver. 5.1): http://physics.nist.gov/asd [2014, June 4]. National Institute of Standards and Technology, Gaithersburg, MD.

Lan, T.-W., Ménard, B., & Zhu, G. 2014, ApJ, 795, 31

Lavalley, M., Isobe, T., & Feigelson, E. 1992, Astronomical Data Analysis Software and Systems I, 25, 245

Madau, P., & Dickinson, M. 2014, ARAA, 52, in press; arXiv:1403.0007

Mannucci, F., Cresci, G., Maiolino, R., Marconi, A., & Gnerucci, A. 2010, MNRAS, 408, 2115

Maoz, D., & Mannucci, F. 2012, PASA, 29, 447

Maoz, D., Mannucci, F., & Brandt, T. D. 2012, MNRAS, 426, 3282

Martin, C. L., Shapley, A. E., Coil, A. L., et al. 2012, ApJ, 760, 127

Ménard, B., & Chelouche, D. 2009, MNRAS, 393, 808

Ménard, B., & Fukugita, M. 2012, ApJ, 754, 116

Menzel, D. H. 1936, ApJ, 84, 462

Morton, D. C. 2003, ApJS, 149, 205

Mshar, A. C., Charlton, J. C., Lynch, R. S., Churchill, C., & Kim, T.-S. 2007, ApJ, 669, 135

Narayanan, A., Charlton, J. C., Misawa, T., Green, R. E., & Kim, T.-S. 2008, ApJ, 689, 782

Nomoto, K., Iwamoto, K., Nakasato, N., et al. 1997, Nuclear Physics A, 621, 467

Oke, J. B. & Gunn, J. E. 1983, ApJ, 266, 713

Oppenheimer, B. D., & Davé, R. 2006, MNRAS, 373, 1265

Prochaska, J. X., Kasen, D., & Rubin, K. 2011, ApJ, 734, 24

Rodríguez Hidalgo, P., Wessels, K., Charlton, J. C., et al. 2012, MNRAS, 427, 1801

Rubin, K. H. R., Prochaska, J. X., Koo, D. C., et al. 2014, ApJ, 794, 156

Savage, B. D., & Sembach, K. R. 1996, ARA&A, 34, 279

Seyffert, E. N., Cooksey, K. L., Simcoe, R. A., et al. 2013, ApJ, 779, 161

Srianand, R. 1996, ApJ, 462, 643

Steidel, C. C. 1995, QSO Absorption Lines, 139

Steidel, C. C., & Sargent, W. L. W. 1992, ApJS, 80, 1

Suresh, J., Bird, S., Vogelsberger, M., et al. 2015, MNRAS, 448, 895

Thielemann, F.-K., Argast, D., Brachwitz, F., et al. 2003, Nuclear Physics A, 718, 139

Torrey, P., Vogelsberger, M., Genel, S., et al. 2014, MNRAS, 438, 1985

Totani, T., Morokuma, T., Oda, T., Doi, M., & Yasuda, N. 2008, PASJ, 60, 1327

Tremonti, C. A., Heckman, T. M., Kauffmann, G., et al. 2004, ApJ, 613, 898

Vogelsberger, M., Genel, S., Springel, V., et al. 2014, Nature, 509, 177

Weiner, B. J., Coil, A. L., Prochaska, J. X., et al. 2009, ApJ, 692, 187

Wiersma, R. P. C., Schaye, J., Theuns, T., Dalla Vecchia, C., & Tornatore, L. 2009, MNRAS, 399, 574

Yanny, B., York, D. G., & Williams, T. B. 1990, ApJ, 351, 377

Yates, R. M., Henriques, B., Thomas, P. A., et al. 2013, MNRAS, 435, 3500

York, D. G., Adelman, J., Anderson, J. E., Jr., et al. 2000, AJ, 120, 1579

Zhu, G., & Ménard, B. 2013, ApJ, 770, 130

Zhu, G., Ménard, B., Bizyaev, D., et al. 2014, MNRAS, 439, 3139